J. Fluid Mech. (2014), *vol.* 755, *pp.* 314–335. © Cambridge University Press 2014
doi:10.1017/jfm.2014.415

Second-order perturbation of global modes and implications for spanwise wavy actuation

O. Tammisola[1,†], F. Giannetti[2], V. Citro[2] and M. P. Juniper[1]

[1]Department of Engineering, University of Cambridge, Trumpington Street, Cambridge CB2 1PZ, UK

[2]DIIN, University of Salerno, via Ponte don Melillo, 84084 Fisciano (SA), Italy

(Received 20 January 2014; revised 24 May 2014; accepted 16 July 2014;
first published online 18 August 2014)

Sensitivity analysis has successfully located the most efficient regions in which to apply passive control in many globally unstable flows. As is shown here and in previous studies, the standard sensitivity analysis, which is linear (first order) with respect to the actuation amplitude, predicts that steady spanwise wavy alternating actuation/modification has no effect on the stability of planar flows, because the eigenvalue change integrates to zero in the spanwise direction. In experiments, however, spanwise wavy modification has been shown to stabilize the flow behind a cylinder quite efficiently. In this paper, we generalize sensitivity analysis by examining the eigenvalue drift (including stabilization/destabilization) up to second order in the perturbation, and show how the second-order eigenvalue changes can be computed numerically by overlapping the adjoint eigenfunction with the first-order global eigenmode correction, shown here for the first time. We confirm the prediction against a direct computation, showing that the eigenvalue drift due to a spanwise wavy base flow modification is of second order. Further analysis reveals that the second-order change in the eigenvalue arises through a resonance of the original (2-D) eigenmode with other unperturbed eigenmodes that have the same spanwise wavelength as the base flow modification. The eigenvalue drift due to each mode interaction is inversely proportional to the distance between the eigenvalues of the modes (which is similar to resonance), but also depends on mutual overlap of direct and adjoint eigenfunctions (which is similar to pseudoresonance). By this argument, and by calculating the most sensitive regions identified by our analysis, we explain why an in-phase actuation/modification is better than an out-of-phase actuation for control of wake flows by spanwise wavy suction and blowing. We also explain why wavelengths several times longer than the wake thickness are more efficient than short wavelengths.

Key words: absolute/convective instability, instability control, wakes/jets

1. Introduction

Control of wake instability by spanwise alternating suction and blowing was studied with direct numerical simulation (DNS) by Kim & Choi (2005). (The alternating

† Email address for correspondence: olot2@cam.ac.uk

https://doi.org/10.1017/jfm.2014.415 Published online by Cambridge University Press

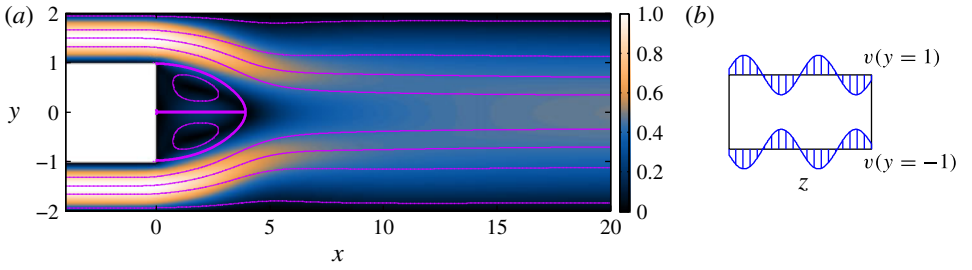


FIGURE 1. (Colour online) (*a*) Base flow: velocity magnitude and streamlines. The boundary of the recirculation bubble is shown by a thick line. (*b*) Illustration of in-phase suction.

suction and blowing will be called 'suction' in the rest of this paper.) Through steady spanwise wavy suction, they shifted the Hopf bifurcation point of the wake behind a cylinder from a Reynolds number of $Re \approx 45$ to $Re = 140$. This degree of stabilization cannot be achieved with any known 2-D open-loop control strategies. Only certain spanwise wavelengths of the actuation were successful in suppressing the instability, however. These wavelengths were approximately 5–6 cylinder diameters. Control at other wavelengths was less effective. The suction was applied from two slots placed on the top and bottom of the cylinder. The configuration in which the suction through the upper slot was in phase with that through the lower slot (figure 1*b*) was found to be much more effective than the antiphase configuration.

In order to explain these effects, Hwang, Kim & Choi (2013) examined the local absolute instability of a fixed streamwise base flow profile (a wake profile), modified sinusoidally in the spanwise direction. The absolute instability was suppressed by spanwise wavy modifications at medium to long wavelengths, while short wavelengths had a strongly destabilizing effect, the latter not observed in the DNS (Kim & Choi 2005). The suppression of absolute instability at medium to long wavelengths was proposed to be based on the interaction of the von Kármán street with vortex tilting.

Very recently, Del Guercio, Cossu & Pujals (2014) examined the effect of streaks in suppressing temporal and absolute instability of wakes. Streamwise streaks were chosen as they are the streamwise uniform perturbations that experience most transient growth around a parallel 2-D wake profile taken as a base flow. The optimal initial condition to create the streaks was shown to be streamwise vortices, as in many shear flows. These optimally amplified streaks were then applied as base flow modifications of the local wake profile, and the temporal and absolute growth rates were recalculated. Del Guercio *et al.* (2014) found that the dependence of the absolute growth rate on the streak amplitudes was quadratic. Furthermore, they suggested that the spanwise wavy modifications are particularly effective as stabilizers because they experience strong transient growth in wake flows. This means that high-amplitude streaks can be created from low-amplitude vortices.

The aim of the present study is to revisit the effect of spanwise wavy steady actuation on stability, using full global analysis of the spatially developing base flow. We explain the findings using a novel generalized sensitivity analysis, which is applicable to spanwise wavy modifications of the base flow and of the linear operator in general. We demonstrate this method on the confined wake behind a flat plate (figure 1). Some of the theoretical results are expected to be directly applicable to the cylinder wake configuration. However, this is not our only aim. The framework

https://doi.org/10.1017/jfm.2014.415 Published online by Cambridge University Press

presented and verified here permits analysis of the effect of spanwise wavy flow perturbations in general (such as streaks), inflow asymmetries in axisymmetric geometries, and control by spanwise wavy actuation.

The second-order terms have not been considered in modal stability studies so far (local or global), to the best of the authors' knowledge. A similar perturbation approach was successfully used in a non-modal study quantifying the effect of streamwise travelling waves on the transient energy growth in a channel flow (Lieu, Moarref & Jovanovic 2010; Moarref & Jovanovic 2010).

2. Perturbation analysis

Let us consider a general eigensystem of the form

$$\mathcal{L}\boldsymbol{q}_0 = \sigma_0 \boldsymbol{q}_0, \tag{2.1}$$

where $\boldsymbol{q}_0$ is an eigenvector and σ_0 is an eigenvalue. We will now perturb the governing operator by another operator $\delta\mathcal{L}$, so that the problem remains a linear eigenvalue problem. Following a standard perturbation approach (e.g. Baumgärtel 1984; Hinch 1991), the problem can be expanded in powers of the perturbation amplitude ϵ:

$$\begin{aligned}(\mathcal{L} + \epsilon\delta\mathcal{L})\{\boldsymbol{q}_0 + \epsilon\boldsymbol{q}_1 + \epsilon^2\boldsymbol{q}_2 + O(\epsilon^3)\} \\ = (\sigma_0 + \epsilon\sigma_1 + \epsilon^2\sigma_2 + O(\epsilon^3))\{\boldsymbol{q}_0 + \epsilon\boldsymbol{q}_1 + \epsilon^2\boldsymbol{q}_2 + O(\epsilon^3)\}.\end{aligned} \tag{2.2}$$

Here, σ_j is the jth order correction to the eigenvalue and $\boldsymbol{q}_j$ ($j > 0$) is the ith order correction to the eigenmode. By grouping the terms at the same order in ϵ, and solving this equation, we will obtain these corrections at different orders.

At the zeroth order in ϵ, the original eigenvalue problem is recovered, satisfied by definition. At the first order in ϵ, we obtain, after rearrangement,

$$(\mathcal{L} - \sigma_0\mathcal{I})\,\{\boldsymbol{q}_1\} = -\delta\mathcal{L}\{\boldsymbol{q}_0\} + \sigma_1\boldsymbol{q}_0, \tag{2.3}$$

where $\mathcal{I}$ is the identity operator. To solve (2.3), we will use the *adjoint* eigenmode $\boldsymbol{q}_0^+$, defined based on an inner product $\langle , \rangle$ such that $\langle \boldsymbol{q}_0^+, \boldsymbol{q}_0 \rangle = 1$. The adjoint is found by solving the eigenproblem for the adjoint operator, $\mathcal{L}^+\boldsymbol{q}_0^+ = \sigma_0^*\boldsymbol{q}_0^+$ (see, e.g., Luchini & Bottaro (2014) for details). The left-hand side has no component in the direction of $\boldsymbol{q}_0$, which can be seen by projecting it onto $\boldsymbol{q}_0$ by $\boldsymbol{q}_0^+$:

$$\langle \boldsymbol{q}_0^+, (\mathcal{L} - \sigma_0\mathcal{I})\,\{\boldsymbol{q}_1\}\rangle = \langle \mathcal{L}^+\{\boldsymbol{q}_0^+\}, \boldsymbol{q}_1\rangle - \langle \boldsymbol{q}_0^+, \sigma_0\boldsymbol{q}_1\rangle = \langle \sigma_0^*\boldsymbol{q}_0^+, \boldsymbol{q}_1\rangle - \langle \boldsymbol{q}_0^+, \sigma_0\boldsymbol{q}_1\rangle = 0, \tag{2.4}$$

where * denotes the complex conjugate. Hence, the right-hand side also must be orthogonal to $\boldsymbol{q}_0^+$ (Fredholm alternative), giving $0 = \langle \boldsymbol{q}_0^+, -\delta\mathcal{L}\{\boldsymbol{q}_0\} + \sigma_1\boldsymbol{q}_0\rangle$, which can be rearranged as

$$\sigma_1 = \langle \boldsymbol{q}_0^+, \delta\mathcal{L}\{\boldsymbol{q}_0\}\rangle. \tag{2.5}$$

This first-order eigenvalue drift is a linear function of the operator perturbation, contains the direct and adjoint eigenmodes, and will lead to the standard sensitivity expressions.

At the second order in ϵ, we obtain from (2.2)

$$(\mathcal{L} - \sigma_0\mathcal{I})\,\{\boldsymbol{q}_2\} = -\delta\mathcal{L}\{\boldsymbol{q}_1\} + \sigma_2\boldsymbol{q}_0 + \sigma_1\boldsymbol{q}_1. \tag{2.6}$$

https://doi.org/10.1017/jfm.2014.415 Published online by Cambridge University Press

By the same argument as for the first order, both the left and the right sides are orthogonal to $\boldsymbol{q}_0$, giving $\sigma_2 = \langle \boldsymbol{q}_0^+, (\delta\mathcal{L} - \sigma_1\mathcal{I})\{\boldsymbol{q}_1\}\rangle$. This leads to

$$\sigma_2 = \langle \boldsymbol{q}_0^+, \delta\mathcal{L}\{\boldsymbol{q}_1\}\rangle. \tag{2.7}$$

We observe that an arbitrary component of $\boldsymbol{q}_0$ can always be added to $\boldsymbol{q}_1$ (Hinch 1991), and that (2.3) would still remain valid. It should be noted that σ_2 remains unaffected by the choice of this component, since $\langle \boldsymbol{q}_0^+, \delta\mathcal{L}\{C\boldsymbol{q}_0\}\rangle - \sigma_1\langle \boldsymbol{q}_0^+, C\boldsymbol{q}_0\rangle = 0$ for any constant C. The choice of C only corresponds to a normalization of the total perturbed eigenvector. A convenient choice to guarantee uniqueness and remove the singularity of the left-hand side in (2.3) is

$$\langle \boldsymbol{q}_0^+, \boldsymbol{q}_1\rangle = C = 0. \tag{2.8}$$

It should be noted that the second-order eigenvalue drift has exactly the same expression as the first-order drift, but with the eigenmode $\boldsymbol{q}_0$ replaced with the first-order eigenmode correction $\boldsymbol{q}_1$. This means that all the sensitivity expressions derived in the literature can be used straight away to obtain second-order corrections, if $\boldsymbol{q}_0$ is replaced by $\boldsymbol{q}_1$. To do this, one of course needs to solve for $\boldsymbol{q}_1$, which can be performed numerically as described in § 4.

2.1. *Application to base flow modifications*

The theory of second-order perturbations up to now is not limited to a particular set of equations. Hereafter, we will limit our consideration to perturbations around a steady state (base flow) of the Navier–Stokes equations, leading to an operator perturbation $\delta\mathcal{L}(\delta\boldsymbol{U})$. A full derivation of the first-order base flow sensitivity can be found in previous works (e.g. Marquet, Sipp & Jacquin 2008), and just a brief version is included here in order for the paper to be self-contained. The total flow field is governed by the incompressible Navier–Stokes and continuity equations,

$$\frac{\partial \boldsymbol{u}_{tot}}{\partial t} + \boldsymbol{u}_{tot}\cdot\boldsymbol{\nabla}\boldsymbol{u}_{tot} = -\boldsymbol{\nabla}p_{tot} + \frac{1}{Re}\nabla^2\boldsymbol{u}_{tot}, \tag{2.9}$$

$$\boldsymbol{\nabla}\cdot\boldsymbol{u}_{tot} = 0, \tag{2.10}$$

where $\boldsymbol{u}_{tot} = (u_{tot}, v_{tot}, w_{tot})$ is a velocity vector, with non-dimensional streamwise (u_{tot}), vertical (v_{tot}) and spanwise (w_{tot}) components, and p_{tot} is the non-dimensional pressure.

In the following, let us denote by capital letters the planar two-dimensional base flow $\boldsymbol{U}(x, y) = [U(x, y), V(x, y)]$, which is obtained by solving the steady two-dimensional Navier–Stokes equations. Around this base flow we consider linear perturbations, denoted by $\boldsymbol{u} = [u, v, w]$. Around a planar base flow, a decomposition into BiGlobal eigenmodes of the following form applies (Theofilis 2003):

$$\begin{aligned}\boldsymbol{u}_0(x, y, z, t) &= \left[\hat{u}_0(x, y, z), \hat{v}_0(x, y, z), \hat{w}_0(x, y, z)\right]\exp(\sigma_0 t)\\ &= \left[\tilde{u}_0(x, y), \tilde{v}_0(x, y), \tilde{w}_0(x, y)\right]\exp(\mathrm{i}\beta_0 z + \sigma_0 t),\end{aligned} \tag{2.11}$$

$$p_0(x, y, z, t) = \hat{p}_0(x, y, z)\exp(\sigma_0 t) = \tilde{p}_0(x, y)\exp(\mathrm{i}\beta_0 z + \sigma_0 t), \tag{2.12}$$

where $\boldsymbol{u}_0 = (u_0, v_0, w_0)$ is a velocity field of the eigenmode, p_0 is its pressure, β_0 is its spanwise wavenumber and σ_0 is its complex temporal eigenfrequency. It should be stressed for later that throughout this paper the superscript $\hat{}$ refers to the whole spatial

https://doi.org/10.1017/jfm.2014.415 Published online by Cambridge University Press

part of the eigenmode including the z-dependence, and $\tilde{}$ is used for the 2-D part. This distinction is important when taking gradients.

By introducing this ansatz into Navier–Stokes equations, and linearizing them, we obtain the BiGlobal generalized eigenvalue problem:

$$\sigma_0 \hat{\boldsymbol{u}}_0 = -\hat{\boldsymbol{u}}_0 \cdot \nabla \boldsymbol{U} - \boldsymbol{U} \cdot \nabla \hat{\boldsymbol{u}}_0 - \nabla \hat{p}_0 + \tfrac{1}{Re} \nabla^2 \hat{\boldsymbol{u}}_0, \tag{2.13}$$

$$\nabla \cdot \hat{\boldsymbol{u}}_0 = 0, \tag{2.14}$$

which we solve with homogeneous Dirichlet boundary conditions for the velocity at all boundaries. The formalism presented for standard eigenvalue problems in the previous section still applies, since it is known that the pressure can be eliminated and hence the generalized eigenvalue problem can be recast into a standard eigenvalue problem. However, the above generalized eigenvalue formulation is convenient to solve numerically.

In what follows, the mode $(\boldsymbol{u}_0, p_0)$ being perturbed will be called the original eigenmode, and its spanwise wavenumber will be denoted by β_0. The spanwise wavenumber of the base flow modification is β_B. The inner product for two velocity vectors $\hat{\boldsymbol{u}}_a$ and $\hat{\boldsymbol{u}}_b$ is here defined as

$$\begin{aligned} \langle \hat{\boldsymbol{u}}_a, \hat{\boldsymbol{u}}_b \rangle &= \lim_{L_Z \to \infty} L_Z^{-1} \int_{-L_Z/2}^{L_Z/2} \int_{D(x,y)} \hat{\boldsymbol{u}}_a^{*\mathrm{T}} \hat{\boldsymbol{u}}_b \, \mathrm{d}x\mathrm{d}y\mathrm{d}z \\ &= \lim_{L_Z \to \infty} L_Z^{-1} \int_{-L_Z/2}^{L_Z/2} \int_{D(x,y)} \left(\hat{u}_a^* \hat{u}_b + \hat{v}_a^* \hat{v}_b + \hat{w}_a^* \hat{w}_b \right) \mathrm{d}x\mathrm{d}y\mathrm{d}z, \end{aligned} \tag{2.15}$$

where $D(x, y)$ is the 2-D flow domain and T denotes the transpose. The adjoint linearized Navier–Stokes operator is defined using the generalized Lagrange identity based on this inner product, with homogeneous boundary conditions for the perturbation, and the adjoint system becomes

$$\sigma_0^+ \hat{\boldsymbol{u}}_0^+ = (\nabla \boldsymbol{U})^{\mathrm{T}} \cdot \hat{\boldsymbol{u}}_0^+ - \boldsymbol{U} \cdot \nabla \hat{\boldsymbol{u}}_0^+ - \nabla \hat{p}_0^+ - \tfrac{1}{Re} \nabla^2 \hat{\boldsymbol{u}}_0^+, \tag{2.16}$$

$$\nabla \cdot \hat{\boldsymbol{u}}_0^+ = 0, \tag{2.17}$$

where it can be shown that $\sigma_0^+ = -\sigma_0^*$, while T denotes a transpose of the nine-component gradient matrix (in tensor notation $[\nabla \boldsymbol{U}^{\mathrm{T}}]_{ij} = \partial U_j / \partial x_i$). The adjoint eigenproblem also has homogeneous Dirichlet boundary conditions.

By imposing a base flow perturbation $\delta \boldsymbol{U}$ onto (2.13) we obtain

$$\sigma_1 = \langle \boldsymbol{q}_0^+, \delta \mathcal{L}(\delta \boldsymbol{U}) \boldsymbol{q}_0 \rangle = \langle \hat{\boldsymbol{u}}_0^+, -\hat{\boldsymbol{u}}_0 \cdot \nabla \delta \boldsymbol{U} - \delta \boldsymbol{U} \cdot \nabla \hat{\boldsymbol{u}}_0 \rangle. \tag{2.18}$$

By integration by parts, and with the homogeneous boundary conditions, the first-order drift is found to be

$$\sigma_1 = \langle \boldsymbol{q}_0^+, \delta \mathcal{L}(\delta \boldsymbol{U}) \boldsymbol{q}_0 \rangle = \langle -\nabla \hat{\boldsymbol{u}}_0^{\mathrm{T}*} \hat{\boldsymbol{u}}_0^+ + \nabla \hat{\boldsymbol{u}}_0^+ \hat{\boldsymbol{u}}_0^*, \delta \boldsymbol{U} \rangle. \tag{2.19}$$

Here, the expression $-\nabla \hat{\boldsymbol{u}}_0^{\mathrm{T}*} \hat{\boldsymbol{u}}_0^+ + \nabla \hat{\boldsymbol{u}}_0^+ \hat{\boldsymbol{u}}_0^*$ is precisely the (first-order) sensitivity to base flow modifications (Marquet *et al.* 2008).

The second-order eigenvalue change with respect to base flow modifications is correspondingly

$$\sigma_2 = \langle \boldsymbol{q}_0^+, \delta \mathcal{L}(\delta \boldsymbol{U}) \boldsymbol{q}_1 \rangle = \langle -\nabla \hat{\boldsymbol{u}}_1^{\mathrm{T}*} \hat{\boldsymbol{u}}_0^+ + \nabla \hat{\boldsymbol{u}}_0^+ \hat{\boldsymbol{u}}_1^*, \delta \boldsymbol{U} \rangle, \tag{2.20}$$

https://doi.org/10.1017/jfm.2014.415 Published online by Cambridge University Press

where $\hat{\boldsymbol{u}}_1$ is the first-order correction to the velocity eigenmode, which can be obtained from

$$-\hat{\boldsymbol{u}}_1 \cdot \nabla \boldsymbol{U} - \boldsymbol{U} \cdot \nabla \hat{\boldsymbol{u}}_1 - \nabla \hat{p} + \frac{1}{Re}\nabla^2 \hat{\boldsymbol{u}}_1 - \sigma \hat{\boldsymbol{u}}_1 = \hat{\boldsymbol{u}}_0 \cdot \nabla \delta \boldsymbol{U} + \delta \boldsymbol{U} \cdot \nabla \hat{\boldsymbol{u}}_0, \quad (2.21)$$

$$\nabla \cdot \boldsymbol{u}_1 = 0. \quad (2.22)$$

2.2. *Wavy base flow modifications*

The first-order eigenvalue correction vanishes for spanwise wavy modifications of 2-D base flows, because the first-order eigenvalue correction is linear with respect to the base flow modification, and hence the total contribution from a z-alternating base flow modification integrates to zero in the z direction. To see this, we consider example base flow modifications of the form $\delta \boldsymbol{U} = \delta \tilde{\boldsymbol{U}}(x, y)\cos(\beta_B z) = \delta \tilde{\boldsymbol{U}}(x, y)[\exp(\mathrm{i}\beta_B z) + \exp(-\mathrm{i}\beta_B z)]/2$. Using (2.15) and (2.19) we obtain

$$\sigma_1 = \left(\lim_{L_Z \to \infty} L_Z^{-1} \int_{-L_Z/2}^{L_Z/2} \cos(\beta_B z)\mathrm{d}z\right) \int_{D(x,y)} \left(-\nabla \hat{\boldsymbol{u}}_0^{\mathrm{T}} \hat{\boldsymbol{u}}_0^{+*} + \nabla \hat{\boldsymbol{u}}_0^{+*} \hat{\boldsymbol{u}}_0\right) \cdot \delta \hat{\boldsymbol{U}}(x, y)\mathrm{d}x\mathrm{d}y = 0, \quad (2.23)$$

because the z-integral vanishes.

The second-order correction σ_2 remains finite, however, because the first-order eigenmode correction is of the form $\boldsymbol{u}_1 = \hat{\boldsymbol{u}}_{1+}(x, y)\exp(\mathrm{i}(\beta + \beta_B)z) + \hat{\boldsymbol{u}}_{1-}(x, y)\exp(\mathrm{i}(\beta - \beta_B)z)$. The reason for this form is that (2.21)–(2.22) are linear, and the wavenumber is uniquely set by the eigenmode and base flow modification through the right-hand side terms. After some algebra we obtain (one should note the inclusion of spanwise gradients)

$$\sigma_2 = 1/2 \int_{D(x,y)} \left(-\nabla \hat{\boldsymbol{u}}_1^{\mathrm{T}} \hat{\boldsymbol{u}}_0^{+*} + \nabla \hat{\boldsymbol{u}}_0^{+*} \hat{\boldsymbol{u}}_1\right) \cdot \delta \tilde{\boldsymbol{U}}(x, y)\mathrm{d}x\mathrm{d}y. \quad (2.24)$$

3. Physical conclusions from the perturbation theory

One can conclude from § 2 that the second-order eigenvalue correction is proportional to the first-order eigenmode correction. Hence, qualitatively, base flow modifications that induce a large eigenmode correction will induce a large second-order eigenvalue drift.

The eigenmode correction is given by (2.21)–(2.22). The left-hand side operator is reminiscent of a resolvent operator. As for a resolvent, there are two ways to obtain a large eigenmode correction: (i) The base flow modification is such that $\hat{\boldsymbol{u}}_1$ is close to an eigenmode of the system (which is similar to modal resonance) or (ii) the base flow modification invokes a large non-modal response (which is similar to pseudoresonance). These properties become obvious when expanding $\hat{\boldsymbol{u}}_1$ in the basis of the original eigenmodes following Hinch (1991): $\boldsymbol{u}_1 = \sum_{N \neq 0} \left[\sigma_0 - \sigma_{(N)}\right]^{-1} \langle \hat{\boldsymbol{u}}_{(N)}^{+}, \delta \mathcal{L} \hat{\boldsymbol{u}}_0 \rangle \hat{\boldsymbol{u}}_{(N)} + C\hat{\boldsymbol{u}}_0$, where N represents a mode index in the original eigenmode basis and C is an arbitrary constant. It should be observed that again $\hat{\boldsymbol{u}}_{(N)}$ refers to the spatial part of the Navier–Stokes eigenmode number N, excluding its time-varying part. It is easily verified that this solution satisfies (2.3), and leads to the following second-order eigenvalue correction:

$$\sigma_2 = \sum_{N \neq 0} [\sigma_0 - \sigma_{(N)}]^{-1} \langle \hat{\boldsymbol{u}}_{(N)}^{+}, \delta \mathcal{L} \hat{\boldsymbol{u}}_0 \rangle \langle \hat{\boldsymbol{u}}_0^{+}, \delta \mathcal{L} \hat{\boldsymbol{u}}_{(N)} \rangle. \quad (3.1)$$

Two restrictions need to be mentioned relating to this expansion.

First, the expansion does not provide physical results in the limit $\epsilon[\sigma_0 - \sigma_{(N)}]^{-1} \approx O(1)$, being in fact singular when $\sigma_{(N)} \to \sigma_0$.

https://doi.org/10.1017/jfm.2014.415 Published online by Cambridge University Press

The singularity occurs because when $\sigma_{(N)} \to \sigma_0$, then $\langle \hat{\boldsymbol{u}}^+_{(N)}, \delta\mathcal{L}\hat{\boldsymbol{u}}_0\rangle\langle \hat{\boldsymbol{u}}^+_0, \delta\mathcal{L}\hat{\boldsymbol{u}}_{(N)}\rangle \to \langle \hat{\boldsymbol{u}}^+_0, \delta\mathcal{L}\hat{\boldsymbol{u}}_0\rangle^2$, which is finite, whereas $[\sigma_0 - \sigma_{(N)}]^{-1} \to \infty$, and therefore $\sigma_2 \to \infty$. In fact, it can be shown that if higher-order corrections are formed, the sum of all eigenvalue corrections will diverge when $\epsilon[\sigma_0 - \sigma_{(N)}]^{-1} \gtrapprox O(1)$. A similar situation occurs, for example, when predicting orbits in a three-planet system (Kolmogorov 1954), yielding a similar expansion with respect to distance. If the orbits of two planets are too close, the perturbation approach becomes invalid and other approaches such as the Kolmogorov–Arnold–Moser (KAM) theory need to be applied. In our case the restriction has the following meaning: the expansion, as well as the perturbation approach itself, is valid as long as the perturbation amplitude is not too large to satisfy $\epsilon[\sigma_0 - \sigma_{(N)}]^{-1} < O(1)$. If two eigenvalues are very close, the perturbation approach is valid only for small perturbation amplitudes.

In the special case of spanwise wavy base flow modifications, this means that when β_B is very close to zero, the sensitivities become arbitrarily large; however, the expansion itself is valid for smaller and smaller amplitudes, and hence conclusions derived from it are of less practical interest in that regime. The reason for the singularity lies in the structure of the eigenmode spectrum for different β. When β is varied, the most unstable eigenvalue is a smooth continuous function of β. Only eigenmodes with wavelength $\beta = \beta_0 \pm \beta_B$ contribute to the sum (3.1). When $\beta_B \to 0$, then $\sigma \to \sigma_0$ for the most unstable mode with $\beta = \beta_0 \pm \beta_B$. The following can be taken as a practical guideline: when the base flow modification amplitude ϵ has been chosen, the theory can be applied for β_B large enough (spanwise wavelength small enough) so that

$$|\sigma_0 - \sigma_{(N)}(\beta_B)| > \epsilon \quad \forall N. \tag{3.2}$$

For $\epsilon = 0.01$ in § 5.3, this translates to the following lower limit for spanwise wavenumber: $\beta_B > 0.15$, whereas for $\epsilon = 0.1$, the upper limit would be approximately $\beta_B > 0.4$.

Second, the eigenvalue that is perturbed needs to belong to the discrete spectrum for the chosen β_0, and a rigorous treatment of the continuous branches in the above sum would require their decomposition into a finite number of discrete 'leaky modes' (Pralits *et al.* 2007).

Despite the two restrictions, the above expansion gives significant insights into the physics of general second-order perturbations, and wavy perturbations in particular, as detailed in § 5.2. Base flow perturbations invoke at the second order a linear resonance between different eigenmodes, similar to the linear frequency response. The eigenvalue drift induced by another eigenmode depends on how close the eigenvalue is to the one being perturbed (modal resonance), and mutual products between adjoint and direct eigenmodes (non-modal effect/pseudoresonance). The two integrands could be large in two different regions of space, and could be affected by two different physical mechanisms, which creates possibilities for rich dynamics. In other words, a non-local base flow modification is not a simple integral of many local base flow modifications. This property is not a consequence of approximations but an inherent physical property of wavy actuation or modification (due to their second-order nature).

4. Numerical solution

The numerical results discussed in the present paper are carried out using two different codes: the finite-element software FreeFem++ (see http://www.freefem.org) and the spectral-element solver (SEM) Nek5000. Three different problems are

https://doi.org/10.1017/jfm.2014.415 Published online by Cambridge University Press

addressed from a numerical point of view: base flow computations (FreeFem++ and Nek5000), eigenmode computations (FreeFem++ and Nek5000) and the computation of the first-order eigenvector correction (FreeFem++).

In FreeFem++, the finite-element method is used to solve the base flow, eigenmode and eigenmode correction equations in § 2. The spatial domain is discretized by a triangular finite-element mesh using a Delaunay–Voronoi algorithm, leading to a mesh with 213 620 triangles and 108 486 vertices. We employ the pair $P2-P1$, consisting of piecewise quadratic velocities and piecewise linear pressure (Taylor–Hood elements), leading to 10^6 degrees of freedom. After derivation of the variational formulation of the governing equations (§ 2), the associated sparse matrices are built by means of the FreeFem++ software.

In FreeFem++, the steady version of (2.9)–(2.10) is solved by the Newton–Raphson iterative procedure to compute the steady base flow for the stability analyses. Second, the direct and adjoint eigenproblems (2.13)–(2.14) and (2.16)–(2.17) are solved using the implicitly restarted Arnoldi method implemented in the ARPACK library (Lehoucq, Sorensen & Yang 1998). Third, the numerical solution of the eigenvector correction $\boldsymbol{q}_1$ is performed, as detailed in a separate section below. All the required matrix inversions are performed using the sparse LU solver UMFPACK (Davis 2004). The iterative procedure is stopped when the L_2 norm of the residual (the latest correction of the Newton iterations) of the governing equations is less than 10^{-7}.

The code chosen for the computation of 3-D (suction-modified) base flows and for the TriGlobal linear stability analysis used for method verification purposes is Nek5000 (Fischer 1997). TriGlobal stability means that the eigenmodes are computed directly from the ansatz $\boldsymbol{u}(x, y, z, t) = \hat{\boldsymbol{u}}(x, y, z)\exp(\sigma t)$, without setting a spanwise wavenumber. For these verification cases, since the aim is to compare stability characteristics, the unmodified 2-D base flow is also computed in Nek5000 and subsequently interpolated into FreeFem++. The spatial discretization for the TriGlobal stability problem (the verification points in figures 3 and 8, and the eigenmode correction verification in figure 6*d–f*) consists of 43 200 spectral elements, with a gradually refined element distribution in the streamwise direction around the downstream edge of the flat plate, and a finer distribution near the walls in the vertical direction. The spanwise direction is discretized by 12 uniformly distributed elements.

Nek5000 is chosen because it allows a highly accurate matrix-free solution of the TriGlobal stability problems in the present work. As for the finite-element method, the incompressible Navier–Stokes equations are cast into a weak form and integrated over the computational domain. A classical Galerkin approximation is used to spatially discretize the governing equations, where each velocity field is related to polynomials two degrees higher than the pressure ($\mathbb{P}_N$–$\mathbb{P}_{N-2}$ formulation). In this work, the polynomial order $p = 5$ was chosen for 3-D computations, and $p = 8$ for the 2-D base flow. The space associated with the velocity is spanned by Nth-order Lagrange interpolants h_i^N, based on a tensor-product grid formed by Gauss–Lobatto–Legendre nodes in each coordinate direction.

The base flows are computed by time stepping the nonlinear Navier–Stokes equations on the same grid as for the stability problem, but using only the upper half of the flow domain. At the centreline, we set a symmetry condition, which eliminates the (antisymmetric) oscillatory modes, and the flow converges towards a steady state. The convergence is considered to be reached when two successive velocity fields, separated by 10 non-dimensional time units, have a maximum absolute difference of 10^{-6}.

https://doi.org/10.1017/jfm.2014.415 Published online by Cambridge University Press

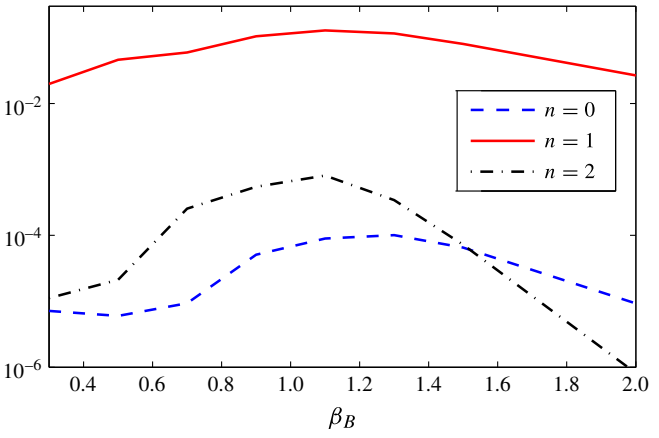


FIGURE 2. (Colour online) The L_2-norm of the first three spatial coefficients $\delta \boldsymbol{U}_n$ of the Fourier transform of the base flow difference $\delta \boldsymbol{U}$, at different suction wavelengths β_B. This shows that the $n = 1$ component ($\propto \exp(\mathrm{i}\beta_B z)$) dominates. The y-scale is logarithmic.

The full three-dimensional eigenpairs of the linearized Navier–Stokes operator are computed (as in Lashgari *et al.* 2014) using the linearized DNS time stepper (available in Nek5000) coupled with the implicit restart Arnoldi method implemented in PARPACK (Maschhoff & Sorensen 1996). Finally, for the 3-D cases, the base flows and base flow modifications (see § 4.1) are extracted from Nek5000 and interpolated into FreeFem++ as follows. To simplify the computational procedure, we assume the base flow modification to be linear with respect to the suction amplitude, and hence have the same wavenumber β_B. If the base flow modification is nonlinear (as it might be for high suction amplitudes), then the base flow modification might contain harmonics at multiples of β_B. Then, a rigorous treatment of these would require extracting the harmonics, and computing eigenvector corrections for each harmonic separately. In figure 2, we have extracted the L_2-norms of the amplitudes of $\exp(\mathrm{i}n\beta_B z)$, $n = 0$, 1, 2, at different β_B. This shows that the components for $n \neq 1$ are smaller by two orders of magnitude compared with $n = 1$, and, hence, it is a good approximation to assume that the base flow difference is of the form $\delta \boldsymbol{U}(x, y) \exp(\mathrm{i}\beta_B z)$. With this assumption, the base flow difference takes the following form:

$$\delta \boldsymbol{U} = \boldsymbol{F}(x, y) \cos(\beta_B z) + \boldsymbol{G}(x, y) \sin(\beta_B z), \tag{4.1}$$

where $\boldsymbol{F} = \delta \boldsymbol{U}(z = 0)$ and $\boldsymbol{G} = \delta \boldsymbol{U}(z = \pi/[2\beta_B])$.

Hence, we interpolate the Nek5000 base flow velocities at $z = 0$ and $z = \pi/(2\beta_B)$ into FreeFem++ and use the above form for the base flow difference. The interpolation proceeds as follows. First, all the $p = 5$ base flows are interpolated in Nek5000 to the Gauss–Lobatto–Legendre points of order $p = 8$ (used for the 2-D base flow). Second, a triangulation is built in FreeFem++ around these points. Third, the base flows are interpolated to the final finite-element grid inside FreeFem++.

4.1. *Second-order perturbation*

Since the solution of the second-order perturbation problem is new, it is worth mentioning the different ways to solve it numerically. There are two ways to obtain

https://doi.org/10.1017/jfm.2014.415 Published online by Cambridge University Press

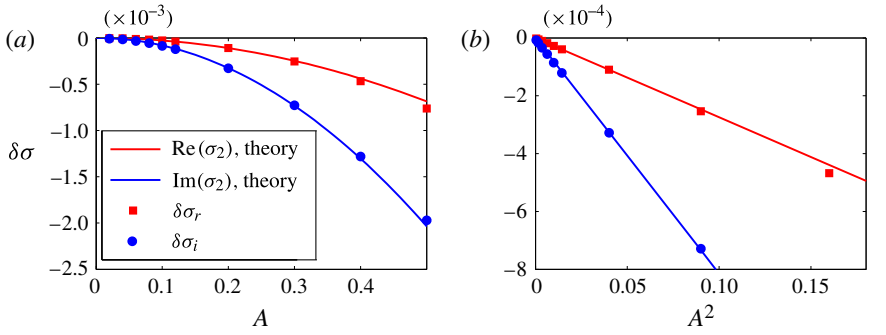


FIGURE 3. (Colour online) (*a*) Markers: the change of the global mode eigenvalue $\delta\sigma = \delta\sigma_r + \mathrm{i}\delta\sigma_i$ as a function of the amplitude A of a given base flow modification (5.1). Solid lines: the predicted eigenvalue perturbation at the second order (σ_2), real and imaginary part. (*b*) The same as (*a*), but as a function of A^2, demonstrating that $\delta\sigma \propto A^2$.

σ_2 for a known operator perturbation (e.g. base flow change). The first is to solve (2.21)–(2.22) directly for $\boldsymbol{u}_1$, and then compute σ_2 from (2.7). The second is to use the eigenmode expansion (3.1) by solving another 2-D global eigenvalue problem, and there is no general rule as to how many modes are needed for the sum to converge.

The choice between the two methods depends on what kind of information is requested. If the exact form of the desired base flow change is known (as in § 5.3, where the base flow change by suction was computed explicitly), then it is clearly preferable to compute the eigenvector correction. If the exact form of the base flow change is unknown, forming the first few terms in the expansion may provide the desired physical insights. In fact, the first term in the sum is a more computationally efficient way to approximate the sensitivity core than traversing a Dirac delta function over the x–y-plane, which will be carried out in § 5.2.

The left-hand side of (2.3) and its specific form (2.21)–(2.22) are singular, as discussed in § 2, which does not affect σ_2 but may place a requirement on the solver. To prevent singularity, we wish to impose the condition $\langle \hat{\boldsymbol{u}}_0^+, \hat{\boldsymbol{u}}_1 \rangle = 0$. This is true whenever $\hat{\boldsymbol{u}}_1$ has a spanwise wavenumber different from β_0. As mentioned in § 2.2, the correct way is to assume that $\boldsymbol{u}_1$ must have the same wavelength as $-\delta\mathcal{L}\{\boldsymbol{u}_0\}$: $\beta_1 = \beta_0 \pm \beta_B$. By replacing $\partial/\partial z$ with $\mathrm{i}\beta_1$ in the equations, we hence automatically impose the above condition, and $(\mathcal{L}(\beta_1) - \sigma_o\mathcal{I})$ becomes non-singular.

The equation system derived from (2.3) becomes

$$\left.\begin{aligned}
&-\hat{\boldsymbol{u}}_{(1,+)}\cdot\nabla\boldsymbol{U} - \boldsymbol{U}\cdot\nabla\hat{\boldsymbol{u}}_{(1,+)} - \nabla\hat{p}_{1,+} + \frac{1}{Re}\nabla^2\hat{\boldsymbol{u}}_{(1,+)} - \sigma\hat{\boldsymbol{u}}_{(1,+)} \\
&\quad = \hat{\boldsymbol{u}}_{(1,+)}\cdot\nabla\delta\boldsymbol{U}_+ + \delta\boldsymbol{U}_+\cdot\nabla\hat{\boldsymbol{u}}_{(1,+)}, \\
&\nabla\cdot\hat{\boldsymbol{u}}_{(1,+)} = 0, \\
&-\hat{\boldsymbol{u}}_{(1,-)}\cdot\nabla\boldsymbol{U} - \boldsymbol{U}\cdot\nabla\hat{\boldsymbol{u}}_{(1,-)} - \nabla\hat{p}_{(1,-)} + \frac{1}{Re}\nabla^2\hat{\boldsymbol{u}}_{(1,-)} - \sigma\hat{\boldsymbol{u}}_{(1,-)} \\
&\quad = \hat{\boldsymbol{u}}_{(1,-)}\cdot\nabla\delta\boldsymbol{U}_- + \delta\boldsymbol{U}_-\cdot\nabla\hat{\boldsymbol{u}}_{(1,-)}, \\
&\nabla\cdot\hat{\boldsymbol{u}}_{(1,-)} = 0,
\end{aligned}\right\} \tag{4.2}$$

where $\partial(\delta\boldsymbol{U}_\pm)/\partial z = \pm\mathrm{i}\beta_B\boldsymbol{U}$, and $\partial\hat{\boldsymbol{u}}_{1,\pm}/\partial z = \mathrm{i}(\beta_0 \pm \beta_B)\boldsymbol{U}$. The base flow change components are found by decomposing the base flow difference as follows:

$$\delta\boldsymbol{U} = \delta\boldsymbol{U}_+ \exp(\mathrm{i}\beta_B z) + \delta\boldsymbol{U}_- \exp(-\mathrm{i}\beta_B z)\,, \tag{4.3}$$

https://doi.org/10.1017/jfm.2014.415 Published online by Cambridge University Press

where $\delta \boldsymbol{U}_+$ and $\delta \boldsymbol{U}_-$ are obtained from (4.1) in a complex form. The above system is solved by the same Newton–Raphson algorithm as the base flow, but the algorithm converges at one iteration because the system is linear. Finally, the second-order perturbation of the eigenvalue was extracted by taking the following integral in FreeFem++:

$$\sigma_2 = \langle -\hat{\boldsymbol{u}}_0^+, \hat{\boldsymbol{u}}_{(1,+)} \cdot \nabla \delta \boldsymbol{U}_- + \delta \boldsymbol{U}_- \cdot \nabla \hat{\boldsymbol{u}}_{(1,+)} + \hat{\boldsymbol{u}}_{(1,-)} \cdot \nabla \delta \boldsymbol{U}_+ + \delta \boldsymbol{U}_+ \cdot \nabla \hat{\boldsymbol{u}}_{(1,-)} \rangle. \quad (4.4)$$

5. Results

To demonstrate the second-order perturbation method, we investigate as an example case the wake behind a flat plate with half-thickness h, confined in a channel of height $4h$. The inflow velocity is parabolic on both sides of the plate. The problem is non-dimensionalized with h and maximum inflow velocity U_{in}. The Reynolds number is fixed at $Re = 100$ for all results presented here. The numerical domain extends from $x = -10$ to $x = 60$ in the streamwise direction, and we employ a no-slip condition at the plate and the channel walls.

5.1. *Verification of quadratic behaviour*

First, we need to show that the eigenvalue drift indeed increases quadratically when the amplitude of the base flow modification is increased; that is, the eigenvalue sensitivity is of second order. Second, we want to compare our predicted eigenvalue drifts with the actual eigenvalue drifts when the base flow is modified and the eigenvalues are recomputed.

For the purpose of this test, we have chosen the same artificially modified 1-D base flow profile as Hwang *et al.* (2013), multiplied by a Gaussian in the streamwise direction:

$$\delta U = A \left[\exp(-(x^2 + 1/2(y-1)^2)) + \exp(-(x^2 + 1/2(y+1)^2)) \right] \cos(z). \quad (5.1)$$

This base flow modification results in a coflow at and around the trailing edge of the plate. It should be noted that this test base flow does not satisfy the Navier–Stokes equations, which is necessary for the sake of method validation. It is impossible to introduce base flow modifications that have exactly the same shape but at different amplitudes, so that the total flow satisfies the Navier–Stokes equations. The procedure is comparable with the addition of optimal streaks to the local base flow profile in Del Guercio *et al.* (2014), with the same shape, but at different amplitudes.

The amplitude of the base flow modification is varied from $A = 0.01$ (1 % of the maximum inlet velocity) to $A = 0.5$ (50 % of the maximum inlet velocity). There is no reason to expect a quantitative agreement at the highest amplitudes even from a second-order prediction. The results are shown in figure 3. The computed changes in both the frequency and the growth rate are clearly quadratic with respect to the amplitude. The quantitive agreement between prediction and computation is almost exact for $A < 0.4$, and as expected deviates more for larger amplitudes. Nevertheless, in particular the frequency component agrees very well even for the largest amplitudes.

5.2. *Sensitivity core for spanwise wavy base flow changes*

Next, we show how the theory can be used not only to predict, but also to physically understand, the influence of spanwise wavy perturbations. In the following, we aim to

https://doi.org/10.1017/jfm.2014.415 Published online by Cambridge University Press

generalize the concept of the wavemaker or the core of the instability for first-order sensitivities (Giannetti & Luchini 2007; Marquet *et al.* 2008), and compare this region for wavy and non-wavy modifications. To do this, we quantify the regions where localized modifications of the base flow similar to a Dirac delta function produce the largest eigenvalue drift. The analogy for first-order sensitivities should not be pushed too far, however. Considering the eigenvalue drift as a sum over eigenmodes as in (3.1), we see that the eigenvalue drifts for large and non-local changes are not obtained from a single integral over many small changes, but rather from a product of two integrals. For a specific global base flow modification, these two integrals could potentially be large in two different regions. Hence, unlike first-order sensitivity base flow modifications, for the second-order perturbations one cannot conclusively obtain all information about the effect of non-local base flow changes from a spatial map obtained for the Dirac delta function.

However, by applying the Dirac delta function we can identify regions where the local flow response for control with each spanwise wavelength is maximum, and hence which are always likely to provide a large contribution. To identify such regions in the flow, to be called 'the sensitivity core', we consider the following highly localized base flow modification:

$$\begin{aligned}\delta U &= B\cos(\beta_B z)\big[\exp(-500((x-x_0)^2+(y-y_0)^2)) \\ &\quad + \exp(-500((x-x_0)^2+(y+y_0)^2))\big], \qquad (5.2)\\ \delta V &= \delta W = 0. \qquad (5.3)\end{aligned}$$

The base flow change is then normalized to a unit area in the x–y-plane by setting the amplitude as

$$B = \left[\int \delta\tilde{U}(x,y)\mathrm{d}x\mathrm{d}y\right]^{-1}. \qquad (5.4)$$

This procedure approximates the effect of a Dirac delta function, but avoids discontinuities which could potentially cause numerical problems.

This base flow modification is traversed over the x–y-plane, and the eigenvalue drift is computed for each (x_0, y_0) pair. Only the streamwise velocity is shown here, but we tried a Gaussian modification of the vertical and spanwise velocities in a few positions too, and these tests indicated that the most efficient regions were similar. The resulting sensitivity core is shown in figure 4. Panel (*a*) shows the standard 2-D sensitivity, (*b*) shows the sensitivity core for $\beta_B = 1$ and (*c*) shows $\beta_B = 30$. This leads to two interesting observations. First, the longer spanwise wavelength ($\beta_B = 1$) causes a larger eigenvalue change than the 2-D modification by a factor of 60 (see the colourbars) and a larger eigenvalue change than the short spanwise wavelength ($\beta_B = 30$) by a factor of two. Second, all three sensitivities are localized along the recirculation bubble and have their maximum at $x \approx 3$–3.5.

A physical explanation for both phenomena – the efficiency of long wavelengths and the similar positions of maximum sensitivity for wavy and non-wavy modifications – is found from the eigenmode expansion (3.1). For spanwise wavy perturbations of wavenumber β_B around a 2-D flow, the base flow sensitivity arises through the mode interactions in the sum (3.1). These only involve modes with $\beta = \pm\beta_B$. No other modes contribute. For a wake behind a flat plate, the most unstable eigenvalue varies continuously as β varies. The eigenvalue spectra at two different values of β are shown in figure 5, together with the 2-D ($\beta = 0$) eigenvalue σ_0 that is being perturbed. At small β (long wavelengths), such as $\beta = 0.3$ ($\lambda = 21$) in figure 5, the leading

https://doi.org/10.1017/jfm.2014.415 Published online by Cambridge University Press

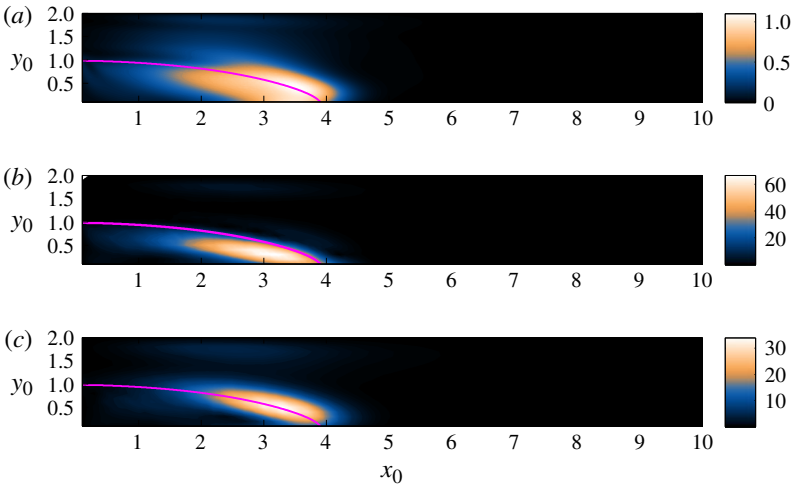


FIGURE 4. (Colour online) The sensitivity core for spanwise wavy base flow modifications estimated by a spatial mapping of the eigenvalue drifts induced by localized modifications approximating a Dirac delta function: (*a*) $\beta_B = 0$ (2-D), (*b*) $\beta_B = 1$, (*c*) $\beta_B = 30$. The eigenvalue drift is large inside the light-coloured region. This demonstrates that when the same base flow modification is applied at different spanwise wavelengths, long wavelengths are more efficient than short ones (see the colourbars) and much more efficient than 2-D suction, while the sensitivity cores have similar shapes to those in 2-D. The boundary of the recirculation zone is depicted by the solid line (magenta online).

eigenvalue is very close to the 2-D eigenvalue ($\beta = 0$), while the other eigenmodes are comparatively far away. Therefore, at small wavenumbers, the interaction between the most unstable mode at $\beta = \pm\beta_B$ and the original mode at $\beta = 0$ provides a large contribution. Qualitatively, the smaller the wavenumber is, the larger the effect on the eigenvalue is (keeping the restrictions of § 3 in mind). Furthermore, the most unstable mode does not change its spatial shape much between $\beta = 0$ and small non-zero β. This means that the sensitivity core remains similar for any small spanwise wavenumber. At slightly larger wavenumbers (such as $\beta_B = 1$ or $\lambda = 6.2$ in figure 5), corresponding to shorter wavelengths, the leading modes are further apart, which means that the effect on σ_0 from the mode interactions is smaller. In this case, other eigenmodes also contribute to the sum, and therefore to the spatial sensitivity distribution, in a similar proportion to the leading mode. However, the wake or shear layer modes that contribute most to the sum have similar frequencies to the wake mode, and these are not essentially different in their spatial distribution, which still gives rise to similar sensitivity regions, but at slightly lower amplitudes.

5.3. *Control effect of steady spanwise wavy suction*

Finally, we apply the theory to study and explain the effect of actual base flow modifications induced by suction on a wake behind a flat plate. A sinusoidal steady wall-normal suction is applied from a slot located near the trailing edge $-0.2 < x < -0.01$, similarly to Kim & Choi (2005): $\boldsymbol{U}_{wall} = (0, 0.01\cos(\beta_B z), 0)$. The suction distributions on the upper and lower surfaces of the plate are in phase with each other (see figure 1*b* for illustration).

https://doi.org/10.1017/jfm.2014.415 Published online by Cambridge University Press

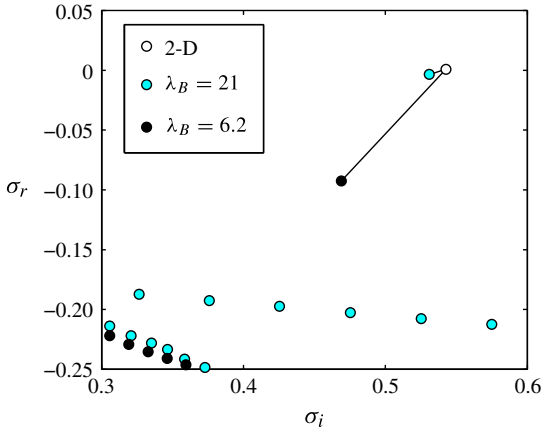


FIGURE 5. (Colour online) Unperturbed eigenvalue spectra for two different spanwise wavelengths ($\lambda_B = 21$ which gives $\beta_B = 0.3$, and $\lambda_B = 6.2$ which gives $\beta_B = 1$), shown together with the unstable 2-D eigenvalue ($\beta = 0$). The solid lines are added to illustrate the distances between the most unstable eigenvalue and the 2-D eigenvalue (white circle). The mode resonance effect (§ 3) is inversely proportional to the distance between eigenvalues.

The choice of an in-phase suction distribution (rather than out-of-phase) is worth mentioning, since this choice turns out to be well grounded in the present theory. In earlier works (Kim & Choi 2005; Hwang *et al.* 2013), in-phase distribution was observed to be much more efficient in stabilizing the flow than out-of-phase distribution, but this effect was not explained. The σ_2 derived in the present work (3.1) contains an integral product of the mode, its adjoint and the base flow change over y. In order for this integral not to vanish, in-phase perturbations may only invoke a resonance of the original mode with sinuous modes, while antiphase perturbations invoke a resonance with varicose modes. The global eigenvalues for varicose modes in wakes are very damped, so the distance between the original eigenvalue and varicose eigenvalues is long. On the other hand, the eigenvalue distance between the original mode and the leading sinuous mode is short, if the spanwise wavelength for suction $\lambda_B = 2\pi/\beta_B$ is long, by the arguments in the previous section. Therefore, the theory shows that long-wavelength in-phase base flow modifications induce the largest eigenvalue drift through the resonance of the original mode with the leading spanwise wavy sinuous mode with wavenumber $\pm\beta_B$.

This in-phase suction is implemented as a boundary condition in the base flow computations for 12 different wavenumbers: β_B = (0(2-D), 0.3, 0.5, 0.7, 0.9, 1.1, 1.3, 1.5, 1.7, 1.9, 2, 30). The difference between the base flows with and without suction is then extracted, as described in § 4. From this point, we proceed in two ways: (i) by computing the eigenvalue change σ_2 based on our theory and (ii) by recomputing the stability around the 3-D modified base flow, to get a reference result. For the computation of σ_2, $\delta\hat{\boldsymbol{U}}(x, y)$ is extracted from the 3-D base flow as described in § 4. The 2-D non-wavy base flow modification is normalized to have the same L_2-norm as the spanwise wavy ones, to ensure a similar suction effort.

The first-order eigenvector correction $\hat{\boldsymbol{u}}_1$ is computed in the process, and this quantity is shown for the first time for linear global modes in figure 6(*a–c*). Both the real and the imaginary parts are computed, and $\hat{\boldsymbol{u}}_1$ is observed to have the following

https://doi.org/10.1017/jfm.2014.415 Published online by Cambridge University Press

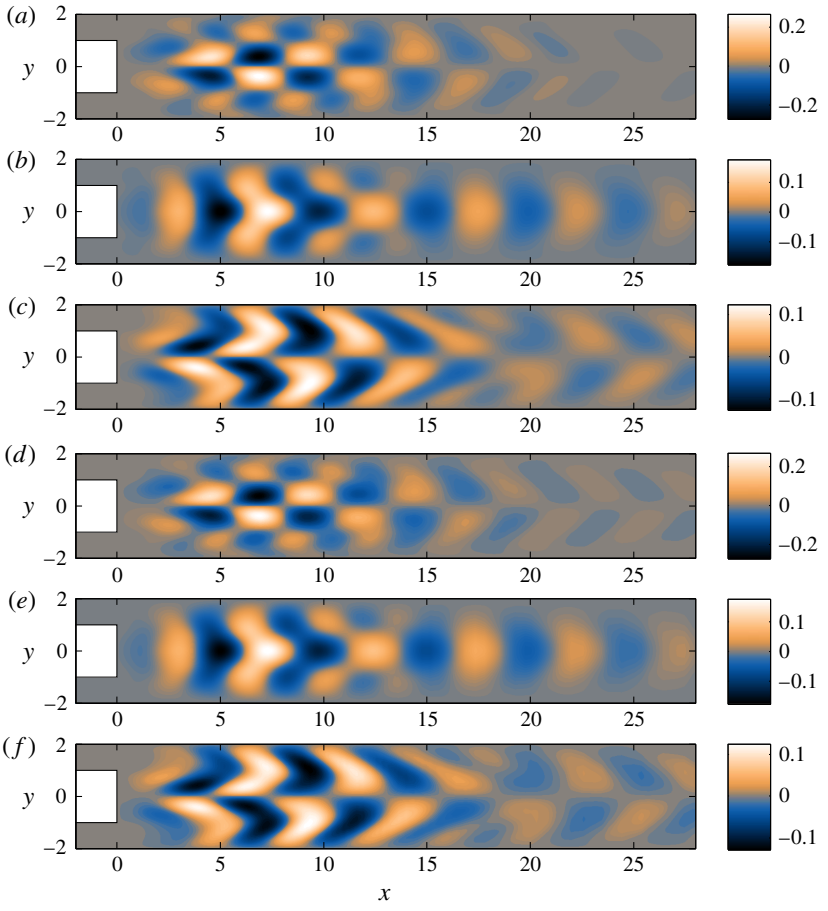


FIGURE 6. (Colour online) (*a–c*) The first-order eigenfunction correction computed from (2.3) with suction wavelength $\beta_B = 1.1$, $\hat{\boldsymbol{u}}_1 = [\tilde{u}_1(x, y)\cos(\beta_B z),\ \tilde{v}_1(x, y)\cos(\beta_B z),\ \tilde{w}_1(x, y)\sin(\beta_B z)]$: (*a*) $\tilde{u}_1$, real part; (*b*) $\tilde{v}_1$, real part; (*c*) $\tilde{w}_1$, real part. (*d–f*) The same as (*a–c*), but where a true eigenfunction correction is extracted from a computed 3-D eigenfunction with suction $\boldsymbol{u}_s$ by subtracting the component in the direction of the unperturbed eigenfunction. Both correction fields are normalized to a unit L_2-norm.

form: $\boldsymbol{u}_1 = \tilde{\boldsymbol{u}}_1(x, y)\cos(\beta_B z)$, $\boldsymbol{v}_1 = \tilde{\boldsymbol{u}}_1(x, y)\cos(\beta_B z)$, $\boldsymbol{w}_1 = \tilde{\boldsymbol{w}}_1(x, y)\sin(\beta_B z)$, following the same symmetry in z as the suction, and the induced base flow modification. The different velocity components are shown in figure 6(*a–c*), for $\beta_B = 1.1$, and these are reminiscent of eigenfunctions of confined wakes, as expected. To further validate our method of computing the eigenvector correction, a true eigenmode correction extracted from a computed 3-D eigenmode is shown in figure 6(*d–f*). The latter result was obtained from a 3-D eigenmode with suction, $\boldsymbol{u}_s$, by subtracting the component in the direction of the original eigenmode: $\boldsymbol{u}_s - \langle \boldsymbol{u}_0^+, \boldsymbol{u}_s \rangle$. The result is nearly indistuingishable from the one computed from our theory. Both corrections are normalized to a unit L_2-norm.

The norm of $\boldsymbol{u}_1$ which will be obtained in an actual computation of an experiment is arbitrary. The reason is worth discussing in some depth. The norm of $\boldsymbol{u}_1$ is uniquely determined by the norm of the unperturbed (original) eigenvector $\boldsymbol{u}_0$. Conversely, when

https://doi.org/10.1017/jfm.2014.415 Published online by Cambridge University Press

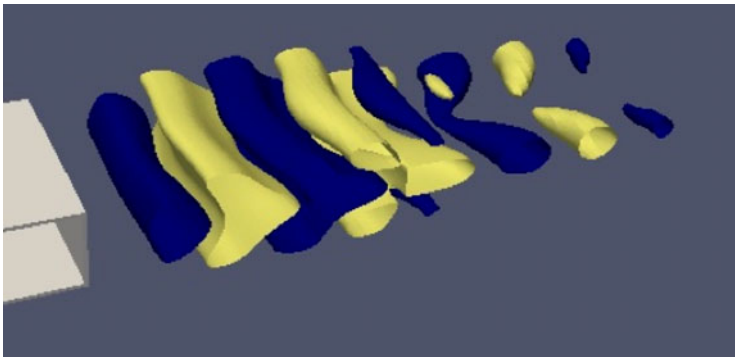


FIGURE 7. (Colour online) The computed triglobal eigenmode with suction, $A = 0.01$ and $\beta_B = 1.1$; positive (dark, blue online) and negative (light, yellow online) contours of the vertical disturbance velocity $\hat{v}_0(x, y, z)$. The edge of the flat plate, extending from $y = -1$ to $y = 1$, is also shown in pale grey.

$\boldsymbol{u}_1$ is known, so that $\langle \boldsymbol{u}_0^+, \boldsymbol{u}_1 \rangle = 0$, then $\boldsymbol{u}_0$ can be determined uniquely by inverting (2.3). However, as mentioned in § 2, an arbitrary component $C\boldsymbol{u}_0$ can always be added to $\boldsymbol{u}_1$ to obtain (non-unique) solutions to (2.3). The actual eigenmode returned from a 3-D computation or an experiment may therefore have any value of C. The value of C can be found from $\boldsymbol{u}_1$, by inverting (2.3), if desired. Importantly, the eigenvalue correction σ_2 remains independent of C, as shown in § 2.

The eigenmode correction has its largest amplitude at $x \approx 5$. However, the relative amplitude of the correction and the original eigenmode determine the final shape, and this depends on the (arbitrary) value of C. Hence, the eigenmode correction observed in computation or experiments might be either small or large, while the observed eigenvalue correction is unique. Figure 7 shows a computed TriGlobal eigenmode with suction. In the shape of the eigenmode, the spanwise variation only shows further downstream (around $x = 8$), where the amplitude of the original 2-D eigenmode is small.

When it comes to changing the eigenvalue, however, neither the shape of the correction nor the original eigenmode can indicate which region in the flow has most influence on the eigenvalue change. To know this, we need to overlap the eigenmode correction with the adjoint original eigenmode and the base flow change induced by suction, as explained in § 2, and as demonstrated later in this section.

Now we turn to the comparison between predicted and computed second-order eigenvalue changes, and the efficiency of different suction wavelengths β_B in influencing the stability of the wake flow. The predicted and computed second-order eigenvalue changes for all but the shortest wavelength are shown in figure 8, demonstrating good qualitative agreement and the same value of the most stabilizing wavelength. The shortest wavelength that we tested, $\beta_B = 30$ ($\lambda_B = 0.2$), is far outside the figure and caused an unobservable change in the eigenvalue for both methods. There are quantitative differences between the computed and the predicted results which were hard to avoid, since they are computed with two different numerical tools, and the base flow difference had to be interpolated from one grid to another. The absolute difference between prediction and computation is small, less than 10^{-3}, and therefore easily influenced by numerics. The eigenvalue difference increases quadratically with suction amplitude, and the growth rate decrease is predicted

https://doi.org/10.1017/jfm.2014.415 Published online by Cambridge University Press

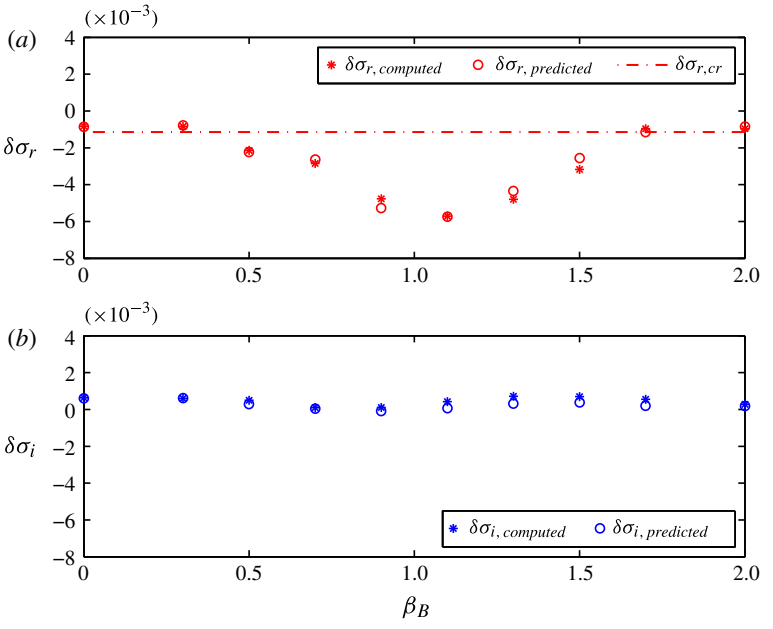


FIGURE 8. (Colour online) The eigenvalue drift for different suction wavenumbers, β_B, for a wake with steady suction where the base flow satisfies the Navier–Stokes equation. Computed and predicted eigenvalue change (see legends): (*a*) change in the real part; (*b*) change in the imaginary part. The value where the growth rate of the suction-modified eigenvalue is zero (neutral stability point) is marked with a dot–dash line in (*a*).

to be $\delta\sigma_r = -0.024$ for only 2 % suction amplitude ($A = 0.02$), and $\delta\sigma_r = -0.15$ for 5 % suction amplitude ($A = 0.05$). We expect the difference between the two numerical tools to be an absolute difference due to the finite accuracy of solution and interpolation, and hence we expect that the relative difference between prediction and computation will be smaller for even slightly larger suction amplitudes.

The growth rate of the eigenvalue decreases slightly for all cases with suction, in both the prediction and the computation. The eigenvalue is stabilized for a wide range of β_B, approximately $0.4 < \beta_B < 1.6$. The maximal stabilization is reached at $\beta_B = 1.1$. This corresponds to a wavelength of approximately 6. The observed optimal wavelengths for a cylinder flow are longer: Kim & Choi (2005) obtained 10–12 in our non-dimensional coordinates, and Hwang *et al.* (2013) 12 in our coordinates. The physical reason for the difference between optimal wavelengths in these two configurations could be the confinement. In previous works (Juniper, Tammisola & Lundell 2011; Tammisola *et al.* 2011), confinement was shown to alter the base flow as well as the structure of the eigenmode at similar Reynolds numbers. Figure 6 indeed seems to show that the eigenmode correction extends all the way to the surrounding walls, as well as the base flow modification induced by suction (figure 9*a–c*), so they might be affected by confinement. However, the principles behind the wavelength selection that we present next are general, and not tied to the specific wake flow in question. First of all, figure 8 shows that the stabilizing influence only occurs for relatively long suction wavelengths, and short wavelengths ($\beta_B > 1.7$) have no effect on the eigenvalue. This is consistent with the results in § 5.2, where a fixed base flow modification $\delta\boldsymbol{U}(x, y)$ was applied with

https://doi.org/10.1017/jfm.2014.415 Published online by Cambridge University Press

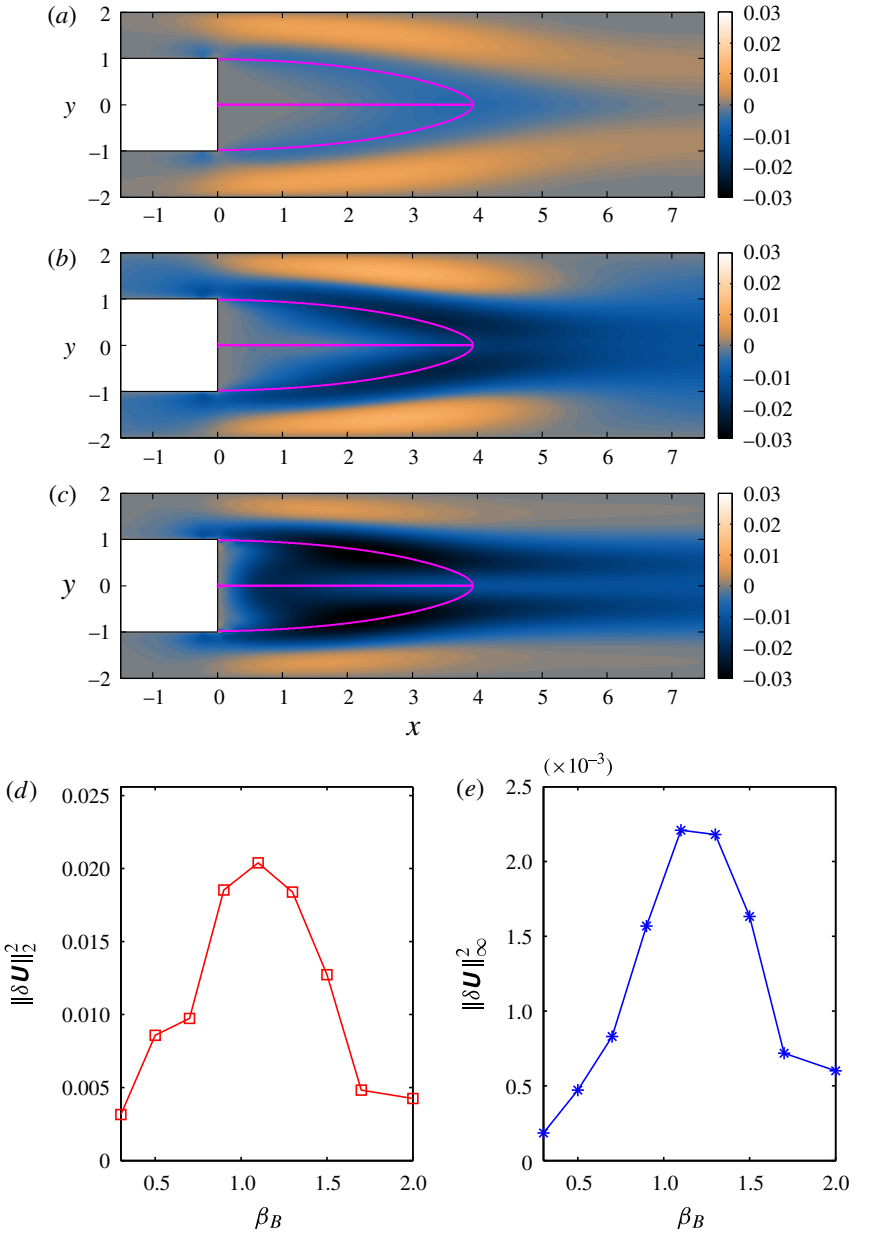


FIGURE 9. (Colour online) The difference between the base flows with and without suction: (*a*) streamwise velocity difference at $\beta_B = 0$ (2-D); (*b*) streamwise velocity difference at $\beta_B = 0.5$ at $z = \pi/(2\beta_B)$; (*c*) streamwise velocity difference at $\beta_B = 2$, $z = \pi/(2\beta_B)$; (*d*) L_2-norm squared as a function of β_B; (*e*) L_∞-norm squared as a function of β_B.

different β_B, and the effect on the eigenvalue decreased with increasing β_B. This also supports the argument presented in § 3 that second-order eigenvalue change can occur due to a resonance between unperturbed eigenmodes at $\beta = 0$ and β_B, when their eigenvalues are close to each other (for illustration see figure 5). The inverse of

https://doi.org/10.1017/jfm.2014.415 Published online by Cambridge University Press

the difference between the most unstable eigenvalues at $\beta = 0$ and β_B is depicted in figure 10(*f*), and explains the general trend that long wavelengths are efficient while short wavelengths are not. However, this argument does not explain why the longest wavelength studied here ($\beta_B = 0.3$) is not stabilizing, and why some slightly shorter wavelengths are performing better. To understand the latter, we consider the structure of the base flow modifications induced by suction.

An important effect was pointed out by Del Guercio *et al.* (2014): the amplitude of the actual base flow change induced by suction is a function of β_B. In figure 9(*a–c*), the streamwise velocity difference between suction and no-suction base flows is shown for $\beta_B = 0$ (*a*), $\beta_B = 0.5$ (*b*) and $\beta_B = 2$ (*c*). Two things can be immediately observed. First, spanwise wavy suction (*b–c*) is clearly more efficient in modifying the base flow than a spanwise invariant suction (*a*). Second, the maximal modification is larger for $\beta_B = 2$ than for $\beta_B = 0.5$. To quantify how efficiently the base flow is modified by suction as a function of β_B, the square of the L_2-norm and the square of the L_∞-norm (maximum norm) of the base flow change are shown for different β_B in figure 9 (the reason for taking the square is that we expect the eigenvalue drift to be proportional to the square of the base flow change). We can see that both base flow changes are maximal at $\beta_B = 1.1$. In particular, the square of the L_2-norm of the base flow change seems to be qualitatively proportional to the growth rate change in figure 8, confirming that this effect plays an important role in selecting the optimal stabilizing wavelength.

It would now be tempting to conclude that the L_2-norm of the base flow change induced by suction, integrated over the whole domain, determines the stability. The region where eigenvalue changes actually occur (where the base flow modification interacts with the eigenmode correction and the adjoint eigenmode) can be shown by plotting the integrand of σ_2, (2.7) or (4.4). In figure 10(*a–d*), this quantity is shown for different β_B. The eigenvalue is only affected by the base flow changes inside the narrow dark region (blue online) in these figures, which follows the edge of the recirculation bubble. For all four suction wavelengths, the base flow changes are seen to influence the flow along the outer edge of the recirculation zone for the 2-D base flow (shown in solid line, magenta online). This effectively coincides with the sensitivity cores shown in § 5.2. The maximum negative value of the integrands (the location in space that contributes to the most stabilizing effect) is in the same location ($x \approx 3.0$, $y \approx 0.6$) for all four wavelengths. In figure 10, we show how the base flow change at the location of maximum sensitivity develops with β_B. This shows the expected trend, with the strongest base flow modification at $\beta_B = 1.1$.

Our conclusion is that two factors combine to determine the optimal wavelength for stabilization of this flow. (i) The eigenmode resonance occurs at long wavelengths. (ii) Medium wavelengths induce largest base flow change inside the sensitivity core region. These competing factors are shown in figure 10(*e*,*f*). Regarding how the base flow change due to suction is created, the reader is referred to the recent paper of Del Guercio *et al.* (2014), where the influence on the cylinder wake base flow is explained to be due to amplification of streaks through the lift-up effect. We expect the same mechanism to be present in this flow, while the base flow changes are slightly modified by confinement.

Finally, it is worth pointing out that the effects described here are based on a global stability analysis, in which the most sensitive region to spanwise wavy perturbations ('sensitivity core') has been identified in the (x, y)-plane, and its location has been related to where the base flow modifications by suction are acting. This was carried out by mapping the effect of a localized base flow modification in the form of a Dirac delta function. Next, by computing the actual base flow modification induced

https://doi.org/10.1017/jfm.2014.415 Published online by Cambridge University Press

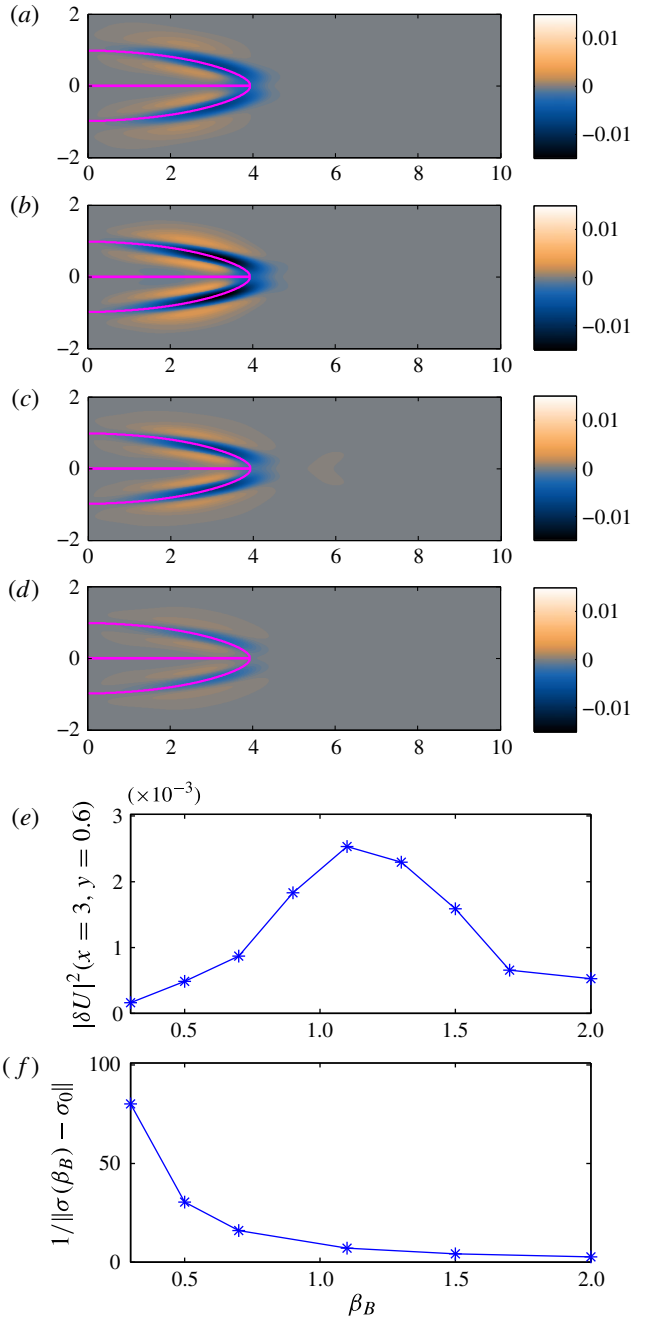


FIGURE 10. (Colour online) (*a*)–(*d*) Integrand of the eigenvalue growth rate change (2.7). Suction wavelengths: (*a*) $\beta_B = 0.7$, (*b*) $\beta_B = 1.1$, (*c*) $\beta_B = 1.5$, (*d*) $\beta_B = 1.7$. A dark colour indicates a stabilizing contribution. The boundary of the recirculation zone of the 2-D base flow is shown by the solid line (magenta online). (*e*) The amplitude of base flow modification at $x = 3.0$, $y = 0.6$, near the maximum negative of the integrands. (*f*) Inverse of the distance from σ_0 to the closest unperturbed eigenvalue at $\beta = \beta_B$.

https://doi.org/10.1017/jfm.2014.415 Published online by Cambridge University Press

by suction, and overlapping this with the product of the adjoint eigenmode and eigenmode correction, we found out where the eigenvalue changes due to suction originate. This turned out to coincide well with the sensitivity core. We did not separate the effects of modifying any specific term in the Navier–Stokes equations. Our arguments for spanwise wavelength selection are hence slightly different from the ones described in the local analysis of Hwang *et al.* (2013), detailing the stabilizing mechanism of a fixed velocity profile. However, the two analyses are not contradictory, as these two mechanisms might coexist in a real flow. Del Guercio *et al.* (2014) point out that spanwise wavy perturbations introduce a base flow change of a large amplitude through the creation of streaks by the lift-up effect. We observe that indeed a 2-D suction induces a smaller global base flow modification than a 3-D spanwise wavy suction, in agreement with Del Guercio *et al.* (2014). However, we extend the previous arguments by identifying the most sensitive region in the x–y-plane, and investigating when the base flow modifications induced by suction are inside this most sensitive region.

The vortex-tilting mechanism described in Hwang *et al.* (2013) might be examined by separating our sensitivities into different components, but this is out of the scope of the present paper. The primary aim here is to present and verify theoretical findings applicable to a much wider class of flow problems involving asymmetric perturbations or control.

6. Conclusions

The sensitivity of global mode eigenvalues has been generalized by considering the eigenproblem perturbation expansion up to the second order. The theory and numerical solution of the derived BiGlobal equation system have been used to shed light on how globally unstable flows are influenced by spanwise wavy actuation, for which the standard sensitivity theory predicts no effect. The computational methods presented for computation of the second perturbations are two-dimensional, except for the base flow with suction which was computed in 3-D (but could also be computed in 2-D as long as the base flow changes linearly with suction amplitude). The 2-D predictions were verified by 3-D computations. The theoretically predicted eigenvalue drift due to spanwise wavy actuation agrees well with the directly computed one. Based on this theory, we argue that the second-order effects on the eigenvalue arise from a resonance between the von Karman eigenmode at infinite spanwise wavelength (2-D) and the same mode at the actuation wavelength. This explains two observations from previous studies: in-phase suction distribution is more efficient than an out-of-phase distribution, and short wavelengths are less efficient than long wavelengths. The optimal wavelength selection is qualitatively explained by showing that the base flow changes induced by suction must be large inside the region most sensitive to spanwise wavy perturbations, called the sensitivity core. From our analysis, this is seen to occur for medium wavelengths. The theory and the eigenmode resonance effect may be relevant to a wide class of problems, for example, the effect of asymmetric inflow profiles on the stability of axisymmetric flows, or flow–acoustics interactions.

Acknowledgements

This work was supported by the European Research Council through Project ALORS 2590620. The work was performed on the computational facilities provided by the Darwin cluster of the University of Cambridge High Performance Computing Service (http://www.hpc.cam.ac.uk/).

https://doi.org/10.1017/jfm.2014.415 Published online by Cambridge University Press

REFERENCES

BAUMGÄRTEL, H. 1984 *Perturbation Theory for Matrices and Operators*, Licensed edition by Birkhäuser Verlag edn. Akademie Verlag.

DAVIS, T. A. 2004 Algorithm 832: UMFPACK, an unsymmetric-pattern multifrontal method. *Trans. Math. Software* **30** (2), 196–199.

FISCHER, P. F. 1997 An overlapping Schwarz method for spectral element solution of the incompressible Navier–Stokes equations. *J. Comput. Phys.* **133**, 84–101.

GIANNETTI, F. & LUCHINI, P. 2007 Structural sensitivity of the first instability of the cylinder wake. *J. Fluid Mech.* **581**, 167–197.

DEL GUERCIO, G., COSSU, C. & PUJALS, G. 2014 Stabilizing effect of optimally amplified streaks in parallel wakes. *J. Fluid Mech.* **739**, 37–56.

HINCH, E. J. 1991 *Perturbation Methods*. Cambridge University Press.

HWANG, Y., KIM, J. & CHOI, H. 2013 Stabilization of absolute instability in spanwise wavy two-dimensional wakes. *J. Fluid Mech.* **727**, 346–378.

JUNIPER, M., TAMMISOLA, O. & LUNDELL, F. 2011 The local and global stability of confined planar wakes at intermediate Reynolds number. *J. Fluid Mech.* **686**, 218–238.

KIM, J. & CHOI, H. 2005 Distributed forcing of flow over a circular cylinder. *Phys. Fluids* **17**, 033103.

KOLMOGOROV, A. N. 1954 On the conservation of conditionally periodic motions under small perturbation of the Hamiltonian. *Dokl. Akad. Nauk SSSR* **74**, 527–530.

LASHGARI, I., TAMMISOLA, O., CITRO, V., BRANDT, L. & JUNIPER, M. P. 2014 The planar *X*-junction flow: stability and control. *J. Fluid Mech.* **753**, 1–28.

LEHOUCQ, R. B., SORENSEN, D. C. & YANG, C. 1998 *ARPACK Users' Guide: Solution of Large-Scale Eigenvalue Problems with Implicitly Restarted Arnoldi Methods*. SIAM.

LIEU, B. K., MOARREF, R. & JOVANOVIC, M. R. 2010 Controlling the onset of turbulence by streamwise travelling waves. Part 2. Direct numerical simulation. *J. Fluid Mech.* **663**, 100–119.

LUCHINI, P. & BOTTARO, A. 2014 Adjoint equations in stability analysis. *Annu. Rev. Fluid Mech.* **46**, 493–517.

MARQUET, O., SIPP, D. & JACQUIN, L. 2008 Sensitivity analysis and passive control of cylinder flow. *J. Fluid Mech.* **615**, 221–252.

MASCHHOFF, K. J. & SORENSEN, D. C. 1996 PARPACK: an efficient portable large scale eigenvalue package for distributed memory parallel architectures. In *Proceedings of the Third International Workshop on Applied Parallel Computing, Industrial Computation and Optimization*, pp. 478–486. Springer.

MOARREF, R. & JOVANOVIC, M. R. 2010 Controlling the onset of turbulence by streamwise travelling waves. Part 1. Receptivity analysis. *J. Fluid Mech.* **663**, 70–99.

PRALITS, J. O., BYSTRÖM, M., HANIFI, A. & HENNINGSON, D. S. 2007 Optimal disturbances in three-dimensional boundary-layer flows. *Ercoftac Bulletin* **74**, 23–31.

TAMMISOLA, O., LUNDELL, F., SCHLATTER, P., WEHRFRITZ, A. & SÖDERBERG, L. D. 2011 Global linear and nonlinear stability of viscous confined plane wakes with co-flow. *J. Fluid Mech.* **675**, 397–434.

THEOFILIS, V. 2003 Advances in global linear instability analysis of nonparallel and three-dimensional flows. *Prog. Aerosp. Sci.* **39**, 249–315.

https://doi.org/10.1017/jfm.2014.415 Published online by Cambridge University Press